J Appl Electrochem (2014) 44:225–232
DOI 10.1007/s10800-013-0633-3

RESEARCH ARTICLE

Morphology and particle growth of a two-phase Ni/Mn precursor for high-capacity Li-rich cathode materials

Jianhong Liu · Hongyu Chen · Jiaona Xie · Zhaoqin Sun · Ningning Wu · Borong Wu

Received: 1 July 2013 / Accepted: 3 October 2013 / Published online: 13 October 2013

Abstract A Ni/Mn composite precursor was prepared as the precursor for Li-rich cathode materials under an air-precipitation atmosphere in a continuous stirred-tank reactor (CSTR). The nucleation and growth of precursor particles were investigated during the CSTR process by monitoring particle morphology, chemical composition, and phase composition. It was found that the particle shape and chemical composition were not homogeneous in the early stages of co-precipitation and did not become so until after 4 h. Mn^{2+} ion oxidation was verified to occur during the entire course of precipitation by X-ray diffraction. The final precipitate was identified as a two-phase system consisting of a Ni/Mn layered double hydroxide phase and a Mn_3O_4 phase. Scanning electron microscopy and an N_2 adsorption–desorption test revealed the porosity and surface area of the material. A Li-rich cathode material was synthesized using the final precipitate as a precursor; the electrochemical performance of this cathode material is reported in this article.

Keywords Ni/Mn composite precursor · Mn^{2+} ions oxidation · Two-phase system · Li-rich cathode material

J. Liu · B. Wu (✉)
School of Chemical Engineering and Environment, Beijing Institute of Technology, Beijing 100081, China
e-mail: borongwu@gmail.com

J. Liu
e-mail: ljh2962@aliyun.com

J. Liu · H. Chen · J. Xie · Z. Sun · N. Wu
CITIC Guoan Mengguli Power Science and Technology Co., Ltd, Beijing 102200, China

1 Introduction

Because of the long endurance mileage and low cost required for rapidly developing electric vehicles, Li-rich solid-solution materials such as $xLi_2MnO_3 \cdot (1-x)LiM_yMn_{(1-y)}O_2$ (M = Co, Ni) have attracted considerable attention as candidates for the cathode in Li-ion batteries because of their high reversible capacity (>200 mAh/g), environmental friendliness, and cheap raw materials [1, 2]. The Li_2MnO_3 component, which integrates into the $LiM_yMn_{(1-y)}O_2$ matrix, effectively restrains the structural collapse of the layered materials at low Li contents and provides high capacity at high operating voltages [3–8].

In order to obtain better cationic distributions, fewer impure phases, and better electrochemical performance in cathode materials, the liquid-state co-precipitation method has been widely used to synthesize the precursor before producing Ni–Mn layered materials [9]. The continuous stirred-tank reactor (CSTR) method can produce particles with more homogeneous compositions and narrower particle-size distributions than can sol–gel and common co-precipitation methods; these advantages of the CSTR method stem from its more controllable feeding speed and reaction speed [10, 11]. The structure, morphology, and electrochemical performance of the hydroxide precursor depend on various synthesis conditions such as the pH, precipitator used, stirring speed, and precipitation atmosphere [12, 13].

If an inert atmosphere is not used during the co-precipitation process—for example, if it is performed in an air atmosphere—then the $Me(OH)_2$ (Me = Ni, Mn) hydroxide may easily oxidize into MeOOH and/or amorphous metal oxide phases [10, 14], yielding a multi-phase mixture as the final product. However, these multi-phase Ni/Mn composites have high catalysis activity because of their

amorphous structure and large surface area; thus, they have been used widely in catalysis [15]. Up to now, few reports have explored particle growth of the spherical-like Ni/Mn hydroxide precursor prepared under an air atmosphere or using these particles to prepare Li-rich material for cathodes in Li-ion batteries.

In this article, a mixed-phase Ni/Mn composite precursor was prepared using the CSTR method under an air atmosphere. The growth course of the precursor was characterized and discussed. By mixing the precursor with a Li source and calcining it at a high temperature, a Li-rich material with a composition of $Li_{1.128}Ni_{0.305}Mn_{0.563}O_2$ was prepared. The electrochemical properties of the cathode material were characterized by scanning electron microscopy (SEM), X-ray diffraction (XRD), and cyclic life testing.

2 Experimental

2.1 Synthesis of the precursor and Li-rich cathode material

The Ni/Mn composite precursor was prepared by co-precipitation of hydrated metal sulfate salts $MnSO_4{\cdot}H_2O$ (AR) and $NiSO_4{\cdot}6H_2O$ (AR) in a basic solution of NaOH at 50 °C in a CSTR under an air atmosphere during the entire precipitation reaction. The theoretical composition of the Ni/Mn composite is $Ni_{0.35}Mn_{0.65}(OH)_2$. The synthesis process was as follows: an aqueous mixed solution of $NiSO_4$ and $MnSO_4$ with a concentration of 2.0 mol/L (Ni:Mn = 0.35:0.65, molar ratio) was pumped into a continuously stirred reactor (feeding rate: 6 ml/min) using digital peristaltic pumps (BT100-2J, Baoding Lange, China). At the same time, a precipitator agent (NaOH solution, 4.0 mol/L) and a chelating agent (NH_4OH, 1.17 mol/L) were separately fed into the reactor at a rate of 6 ml/min. The NaOH and NH_4OH solution pumping was automatically controlled by the pH controller (HANNA, pH500221-2, Italy). A pH of around 10.5 was maintained during the entire precipitation reaction. The temperature (50 °C) and stirring speed (1,000 rpm/min) in the reactor were carefully controlled. At the beginning of the reaction, simultaneously adding the precipitator NaOH solution and the Ni/Mn salt solution into the reaction tank caused a yellow precipitate to appear; the color of the precipitate then gradually changed to brown and then to puce as the reaction proceeded. At the end of reaction a nearly black precipitate was obtained.

The precursor was periodically collected during the course of the experiment. The collected samples were washed with deionized water three times to eliminate residual sodium and sulfuric species; then these samples were subjected to an ethanol exchange operation before drying the products inside a vacuum oven at 80 °C for 8 h. After precipitation reaction finished, the dried precipitate was mixed with Li_2CO_3 (AR) at predetermined elemental ratio of $0.3Li_2MnO_3{\bullet}0.7LiMn_{0.5}Ni_{0.5}O_2$ and calcined at 900 °C for 10 h in air to obtain the final cathode material.

2.2 Characterization and electrochemical test of powders

The particle morphologies of the samples were characterized using field-emission SEM (FESEM) on a Hitachi S-4800 (Japan). Energy-dispersive X-ray spectroscopy (EDS) was used to qualitatively test the Mn/Ni atomic ratio of the collected precursors. The average composition of each sample was determined by EDS measurements of many particles. XRD patterns of samples were collected on a Bruker D8 ADVANCE powder diffractometer (Germany) with Cu Kα radiation ($\lambda = 1.5406$ Å) between 10° and 90° (40 kV, 40 mA, step size = 0.02° and count time of 0.2 s/step) to identify the crystalline phases of the materials. Rietveld refinements of the XRD patterns were performed using Bruker Topas 4.2 software. Nitrogen adsorption–desorption isotherms of the final precipitate was recorded at 77 K on a V-Sorb 2800P (Gold APP. Co. Ltd., Beijing, China). The powder was baked at 130 °C overnight prior to N_2 adsorption. The specific surface area was calculated by the Brunauer–Emmett–Teller (BET) method using a relative pressure (P/P_0) range of 0.081–0.208. The pore-size distribution was determined with the Barrett–Joyner–Halenda algorithm using the adsorption branch. The chemical composition of each sample was analyzed by inductively coupled plasma mass spectrometry (ICP-MS, ElanDRCII, Perkin Elmer, USA).The particle-size distributions of the powders were identified by a laser particle-size analyzer (Beckman LS32, USA).

The electrochemical performance of the prepared cathode material was evaluated in CR2032-type coin cells. Electrodes were made by casting a slurry of 90 % weight active material, 5 % conductive reagent (Timcal, super-P), and 5 % PVDF binder (Kynar, 761A) in an *N*-methyl-2-pyrollidinone solvent onto an Al foil substrate. The slurry was cast by doctor blade. The cast laminates were first dried in air at 120 °C for 2 h and then in a vacuum at 70 °C for 8 h. They were then pressed to thicknesses of 80–100 μm, each electrode having the same weight of active material (~7.26 mg). Lithium coin cells were fabricated in an Ar-filled glove box (<1 ppm O_2) with lithium metal as the anode, Celgard 2400 microporous polypropylene membrane as the separator, and 1 M of $LiPF_6$ in a 1:1:1 volume-fraction mixture of ethylene carbonate, dimethyl carbonate, and ethyl–methyl carbonate as the electrolyte. The charge–discharge performance characteristics of the coin cells were investigated using a CT2001A battery tester (Land, Wuhan, China) at 25 °C.

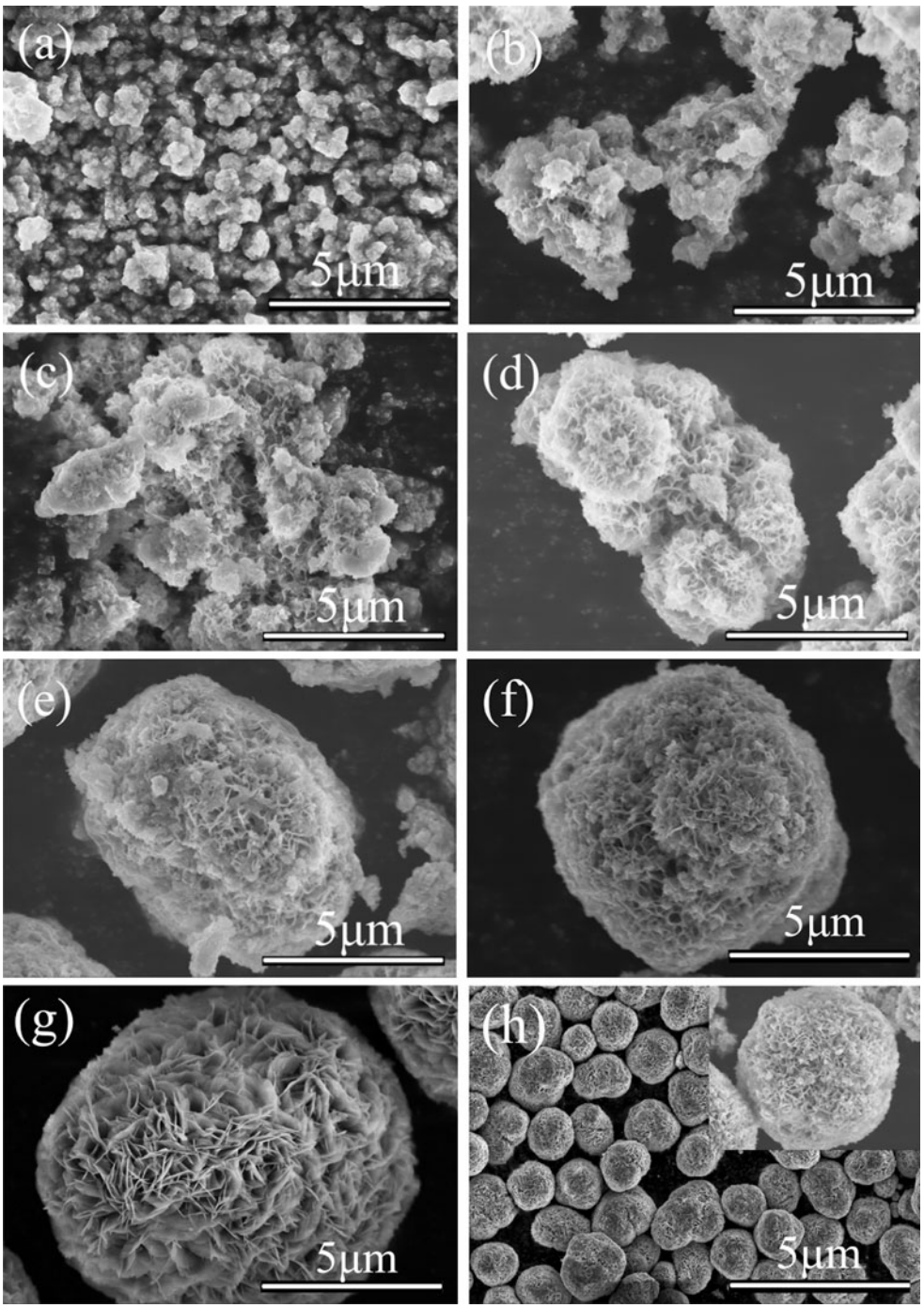

Fig. 1 SEM morphologies of samples collected at different reaction times: **a** 15 min, **b** 45 min, **c** 60 min, **d** 90 min, **e** 180 min, **f** 240 min, **g** 300 min, and **h** 480 min

3 Results and discussion

Figure 1 shows SEM images of the precursors collected during the CSTR experiment, revealing their morphologies. These images show the trend of particle nucleation and growth during the co-precipitation process. During the first phase (15 min) of the reaction, the precursor particles are composed of loose agglomerates with no definite shape. Over time, some larger agglomerates of different sizes form. After 90 min, obvious segregation and agglomeration occurs until the particles become sphere-like as they continue to grow. The surfaces of the final particles are obviously porous with petal-shaped components.

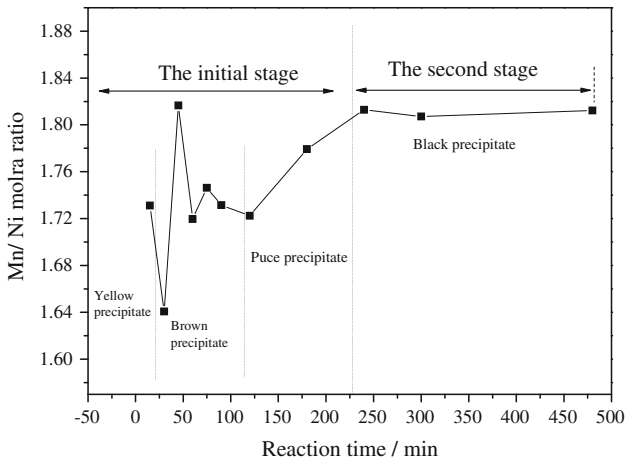

Fig. 2 Mn/Ni molar ratios of precursors obtained by EDS

Figure 2 shows the Mn/Ni ratios of samples collected during co-precipitation, measured using EDS. Qualitative analysis of the samples shows that the Mn/Ni molar ratio varies in the early stages of co-precipitation, stabilizing after ~4 h of reaction. During the initial stages of co-precipitation, the intended and measured Mn/Ni atomic ratios differ greatly and the color of the precipitate gradually changing from yellow to puce. This phenomenon might be attributed to oxidation of Mn^{2+} ions in the precipitate. As the reaction proceeds, the Mn/Ni atomic ratio increases and comes to a steady state after ~4 h of reaction (the second stage). The exact Mn/Ni molar ratio in final precipitate was measured to be 1.845 by ICP method, which is lower than the intended value of 1.8571. This result indicates that a small quantity of the Mn source was not deposited during the co-precipitation reaction, which may have been caused by the larger hydrolyzation equilibrium constant of $Mn(OH)_2$ compared with $Ni(OH)_2$ during the precipitation reaction [16].

Figure 3a shows XRD patterns of samples collected during co-precipitation. The magnified XRD curves of samples collected at 15 and 480 min are shown in Fig. 3b. These diffractograms show a layered structure of Ni/Mn layered double hydroxide (LDH) compounds, consistent with earlier reports [14, 17, 18]. The Bragg peak at 11.5° and 22° can be indexed as the diffraction pattern of the (003) and (006) crystal faces of the LDH phase, respectively. The broad peaks can be believed to be caused by the small average grain size and microstrain in the structure. The many sharp peaks highlighted by the square symbols in Fig. 3 are well indexed to the Mn_3O_4 phase. The presence of the Mn_3O_4 phase in the precipitate can be attributed to Mn^{2+} oxidizing to a higher valence in the air atmosphere, which agrees with earlier reports [10, 14, 15]. As Fig. 3 shows, the oxidation of Mn^{2+} ions continues throughout the entire co-precipitation process. Based on these XRD results, the precipitate was identified to be a two-phase system consisting of Ni/Mn LDH and Mn_3O_4. Unlike the micro-morphologies of the particles, which continually change throughout the co-precipitation process, the phase composition of the precipitate does not change as the precipitation reaction proceeds.

For precursors composed of mixed transition metals, the chemical homogeneity of the final cathode preparation is important. The elemental distribution of the final precipitate is shown in Fig. 4. The transition metals are well distributed; the slight differences in the strengths of the mapping traces are caused by differences between the X-ray scattering factors of Mn and Ni.

The particle-size distributions of samples at different reaction times are shown in Fig. 5a. In the initial stage (15 min), the particle distribution was anomalously broad, ranging from 0.5 to 300 μm. The large particles can be thought as agglomerations of many small particles. As the co-precipitating reaction continued, the particle-size distribution gradually becomes narrow, and the distribution maximum shifted to high value. The average particle size (D50) is shown in Fig. 5b. During the first 45 min of reaction, the D50 value fluctuated without a discernible trend. As the reaction continued, the D50 value increased rapidly, which corresponds with seeded nucleation and growth. From 300 to 480 min, the acceleration of D50 value decreased. A possible explanation for this behavior is that equilibrium might have been gradually reached between nucleation and segregation when the solution was stirred strongly.

Figure 6 shows the results of nitrogen adsorption/desorption experiments performed on the final precipitate. It can be seen that the N_2 adsorption/desorption curve has a type IV-like isotherm, characteristic of microporous materials. The specific surface area calculated from the BET method is 35.4 m^2/g, confirming the porous structure of the particles. The pore-size distribution (Fig. 6, inset) is non-normal, and the maximum radius of the pore-size distribution obtained by the Barrett–Joyner–Halenda algorithm is 2.25 nm.

After lithiating the precursor, a Li-rich cathode material was prepared at a high temperature. The real composition of the Li-rich material was identified by the ICP method as $Li_{1.128}Ni_{0.305}Mn_{0.563}O_2$. Figure 7 shows the XRD pattern of $Li_{1.128}Ni_{0.305}Mn_{0.563}O_2$. All of the diffraction peaks are indexed based on a hexagonal α-$NaFeO_2$ structure with an *R-3m* space group. The peaks between 20° and 23°, highlighted by the arrows in Fig. 7, are identified as the (020) and (110) reflections of the super-lattice structure of the Li_2MnO_3-like component (*C2/m* space group), as many reports have demonstrated

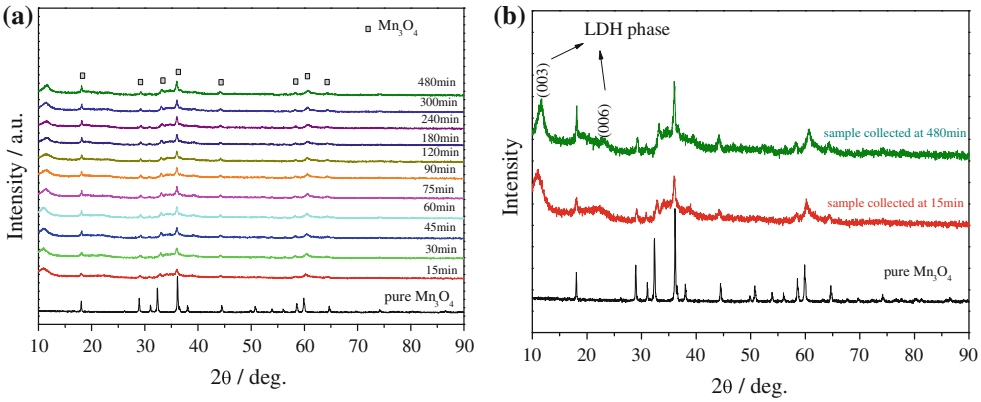

Fig. 3 XRD patterns of the samples collected during the co-precipitation process

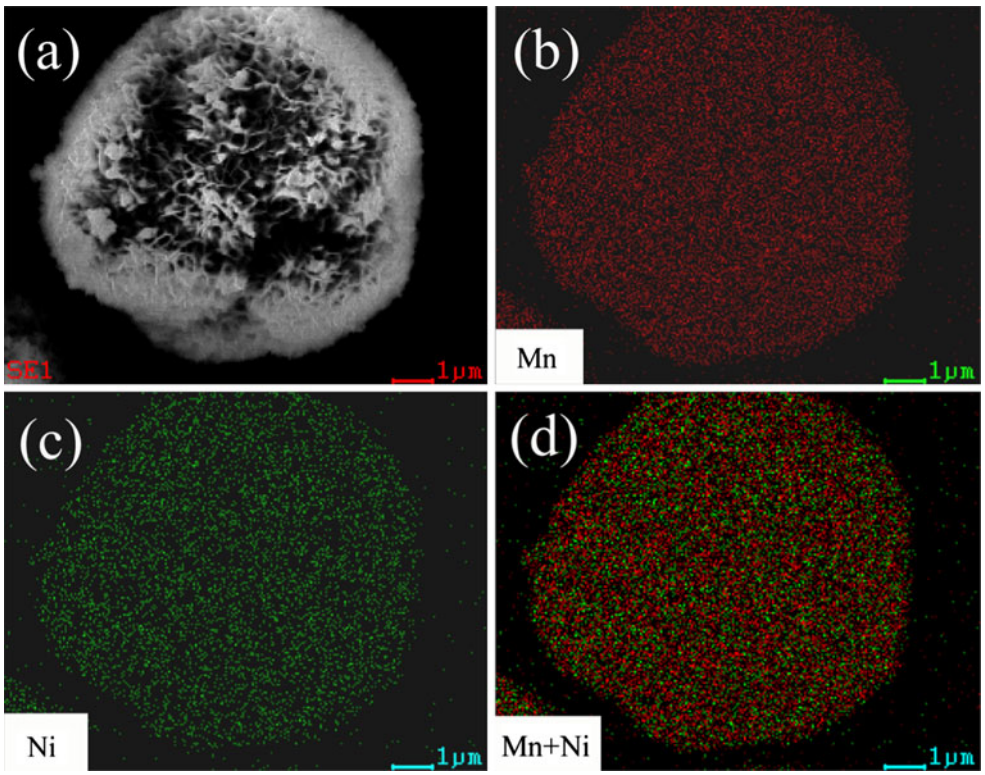

Fig. 4 SEM maps of Mn and Ni ions obtained by EDS: **a** SEM photo of one particle, **b** Mn elemental map, **c** Ni elemental map, and **d** composite map of Mn and Ni

[19–23]. According to earlier reports, the prepared $Li_{1.128}Ni_{0.305}Mn_{0.563}O_2$ material in this work also can be written using the formula: $xLi_2MnO_3{\cdot}(1-x)LiNi_{0.5}Mn_{0.5}O_2$ ($x \sim 0.3$) [4]. The lattice parameters of $Li_{1.128}Ni_{0.305}Mn_{0.563}O_2$ were calculated using Rietveld refinements based on the *R-3m* space group; these values are listed in Table 1. The high *c*/*a* of 4.976 (larger than 4.899) indicates an explicit crystalline for layer structure [24]. The distinct splits in the (006)/(102) and (108)/(110) peaks further support the presence of a well-layered structure in the as-prepared material. In addition, because the I_{003}/I_{104} ratio of 1.3654 is larger than 1.2, this material contains little Li^+ or Ni^{2+} disordering. The *R* factor of $(I_{006}+I_{102})/I_{101}$ is 0.3762, which also supports the presence of a well-ordered structure [25]. Thus, a Li-rich cathode material with a well-ordered layered structure was successfully synthesized from a Ni/Mn precursor with mixed phases. The Mn_3O_4 phase oxidized

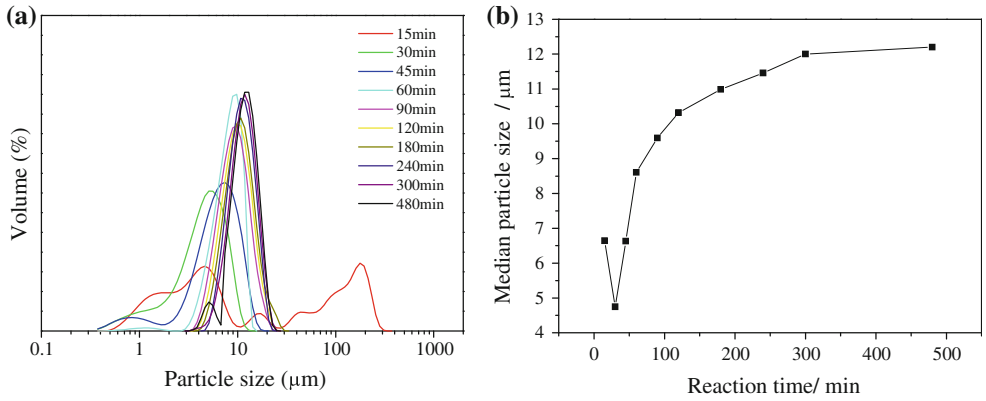

Fig. 5 Particle size evolution as a function of reaction time: **a** particle-size distribution and **b** median particle size

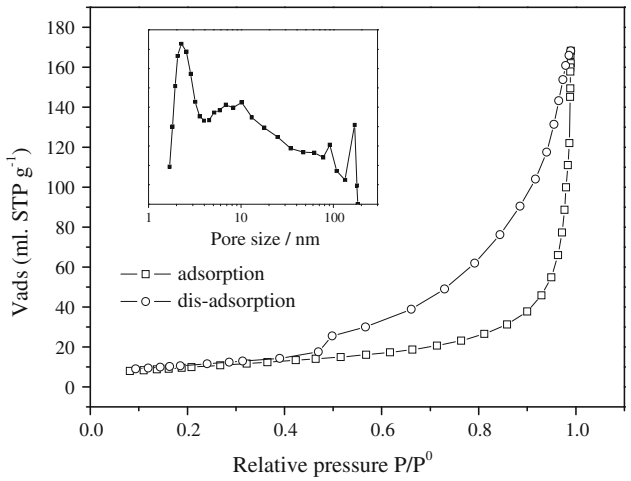

Fig. 6 Pore structure characterization of the particles in the final precipitate

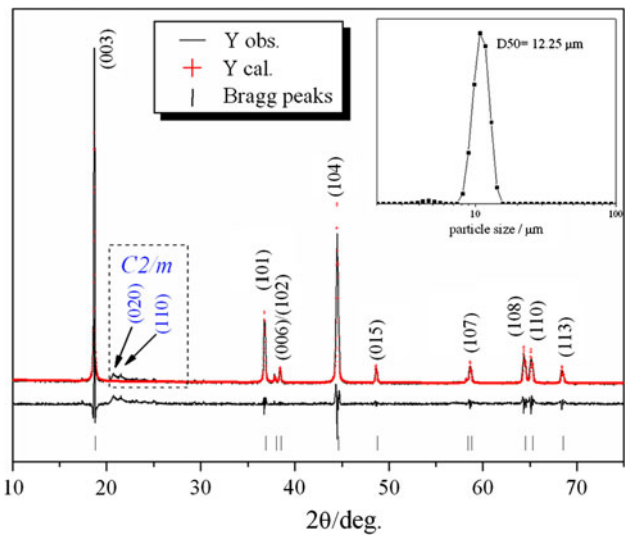

Fig. 7 Observed and calculated X-ray Rietveld refined patterns of prepared $Li_{1.128}Ni_{0.305}Mn_{0.563}O_2$ are shown using a continuous line and a cross sign, respectively. $R_{wp} = 11.21$. The *inset* shows the particle-size distribution curve

from Mn^{2+} in the precursor does not affect the formation of the Li_2MnO_3-like phase in the final solid-solution material.

Figure 8 shows SEM images of the morphology of the final as-prepared Li-rich cathode material, $Li_{1.128}Ni_{0.305}Mn_{0.563}O_2$. The powder is composed of relatively regular spherical particles with diameters of ~10–20 μm. Figure 8b shows a magnified photo of a single particle. The particles have a porous, loose structure of smaller primary particles, which are about 300 nm in diameter. These micrographs suggest that the very porous structure remains after the material is lithiated. The specific surface area of the $Li_{1.128}Ni_{0.305}Mn_{0.563}O_2$ obtained by the BET method is 6.4 m^2/g. The reduction in specific surface area can be attributed to the primary particles fusing to each other during high-temperature calcination, generating larger primary particles.

Figure 9 shows the first charge and discharge profile of $Li_{1.128}Ni_{0.305}Mn_{0.563}O_2$ in a half-cell configuration. The current density was 25 mA/g, which is equivalent to a 0.1 C rate assuming the theoretical reversible capacity to be 250 mAh/g. The cell was initially charged to 4.8 V and then discharged to 2 V. During the first charge, the initial capacity of 141.1 mAh/g observed below 4.4 V can be attributed to the oxidation of Ni^{2+} to Ni^{4+} in the $LiNi_{0.5}Mn_{0.5}O_2$ component of the solid–solution material [7, 26, 27]. According to previous reports, the capacity of 181.7 mAh/g observed in the plateau region between 4.4 and 4.8 V correlates with Li_2O extraction from the Li_2MnO_3 component [3–8]. The discharge capacity during the first cycle is 237.04 mAh/g with a columbic efficiency of 76 %. The prepared material exhibits a relatively high drain performance of 211 mAh/g (87 % of the 0.1 C capacity) at a 1 C discharge rate and 177 mAh/g (70 % of the 0.1 C capacity) at a 3 C discharge rate, as shown in Fig. 10. The stable discharge capacity of 177 mAh/g at a 3 C rate was retained for about 100 cycles.

Table 1 Structural parameters of the final material synthesized by the Ni/Mn precursor with mixed phases

Chemical formula	a (Å)	c (Å)	c/a	I_{003}/I_{104}	$(I_{006} + I_{102})/I_{101}$
$Li_{1.128}Ni_{0.305}Mn_{0.563}O_2$	2.8643	14.2532	4.976	1.3654	0.3762

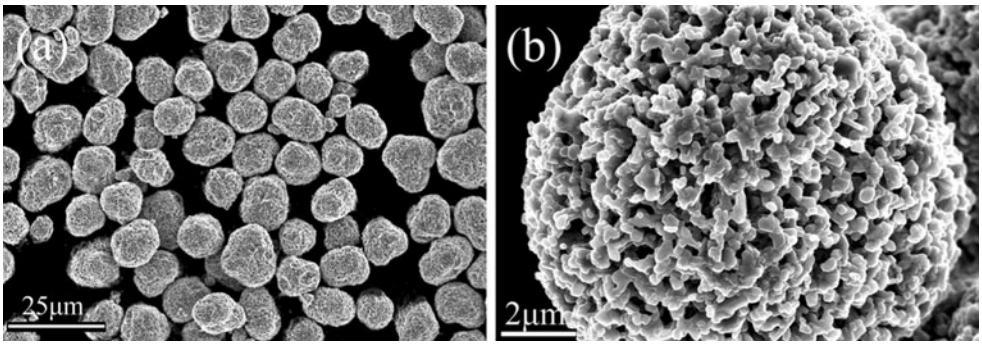

Fig. 8 SEM images of the morphology of the prepared cathode material $Li_{1.128}Ni_{0.305}Mn_{0.563}O_2$: **a** overview of particle morphology and **b** magnified micrograph of a single particle

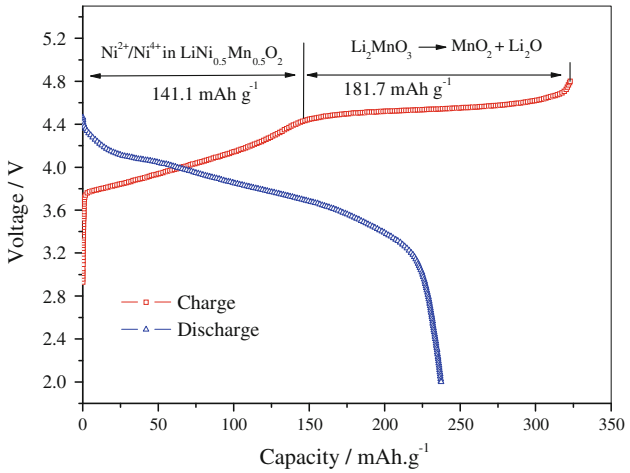

Fig. 9 The first charge–discharge curves of the Li-rich material at a 0.1 C rate

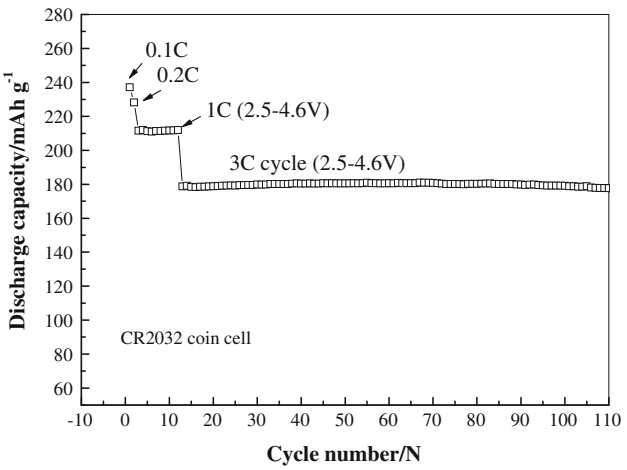

Fig. 10 Cyclic profile taken at room temperature of the prepared $Li_{1.128}Ni_{0.305}Mn_{0.563}O_2$ material. In the first two cycles, the charge rate of is 0.1 C; the charge–discharge voltage range is 2.0–4.8 V

4 Conclusions

A Ni/Mn precursor was prepared using co-precipitation under an air atmosphere. XRD and SEM results confirmed that the nucleation and growth process began with the formation of a two-phase mixture consisting of Ni/Mn LDH and Mn_3O_4. It had been confirmed that Mn^{2+} oxidation proceeded during the entire course of precipitation. The co-precipitation reaction started with the formation of irregularly shaped seed particles with fluctuating chemical stoichiometries and ended with the precipitation of flower-like, spherical homogeneous particle composites composed of two phases. EDS results indicated that Mn^{2+} oxidation during precipitation did not affect the homogeneous element distribution of Ni and Mn in the final precursor particles. The precursor particles continued growing through the CSTR reaction and reached a final average diameter of 12.25 μm. The final precursor particles had a petal-like structure and high surface area. By lithiating the precursor at a high temperature, a Li-rich solid-solution phase cathode material was synthesized. The Li-rich cathode material retained a very porous structure with a relatively small primary particle size of about 300 nm and exhibited relatively stable cyclic performance.

Acknowledgments This work was financially supported by the National High-Tech Research and Development (863) Plan of China (No. 2011AA11A230). The authors would like to thank Ms. Lin Li (CFQS, China) for ICP test discussions and Mr. Xia Weimin (Ametek. Co. Ltd, Shanghai, China) for EDS test discussions.

References

1. Johnson CS, Li N, Lefief C, Vaughey JT, Thackeray MM (2008) Chem Mater 20:6095
2. Bareno J, Lei CH, Wen JG, Kang SH, Petrov I, Abraham DP (2010) Adv Mater 22:1122
3. Wu Y, Manthiram A (2008) J Power Sour 183:749
4. Johnson CS, Li N, Lefief C, Vaughey JT, Thackeray MM (2007) Electrochem Commun 9:787
5. Yu LY, Qiu WH, Huang JY, Lian F (2009) Mater 16:458
6. Kim GY, Yi SB, Park YJ, Kim HG (2008) Mater Res Bull 43:3543
7. Johnson CS, Kim JS, Lefief C, Li N, Vaughey JT, Thackeray MM (2004) Electrochem Commun 6:1085
8. Lim JH, Bang H, Lee KS, Amine K, Sun YK (2009) J Power Sour 189:571
9. Kim JM, Kumagai N, Chung HT (2006) Electrochem Solid-State Lett 9:A494
10. Park SH, Kang SH, Belharouak I, Sun YK, Amine K (2008) J Power Sour 177:177
11. Lee KS, Myung ST, Bang HJ, Chung S, Sun YK (2007) Electrochim Acta 52:5201
12. Song QS, Tang ZY, Guo HT, Chan SLI (2002) J Power Sour 112:428
13. Chang XP, Zhang X, Chen N, Wang K, Kang LP, Liu ZH (2011) Mater Res Bull 46:1843
14. Zhao XM, Zhou F, Dahn JR (2008) J Electrochem Soc 155:A642
15. Tang QH, Wu CM, Qiao R, Chen YT, Yang YH (2011) Appl Catal A 403:136
16. Chen Z (2002) Chem Geol 188:23
17. Kovanda F, Grygar T, Dornicak V (2003) Solid State Sci 5:1019
18. Zhou F, Zhao XM, Bommel AV, Rowe AW, Dahn JR (2010) Chem Mater 22:1015
19. Thackeray MM, Johnson CS, Vaughey JT (2005) J Mater Chem 15:2257
20. Robertson AD, Bruce PG (2003) Chem Mater 15:1984
21. Kang SH, Park SH, Johnson CS, Amine K (2007) J Electrochem Soc 154:A268
22. Belharouak I, Koenig GM, Ma J, Wang DP, Amine K (2011) Electrochem Commun 13:232
23. Lin J, Mu D, Jin Y, Wu B, Ma Y, Wu F (2013) J Power Sour 230:76
24. Shaju KM, Subba GV, Chowdari BVR (2002) Electrochim Acta 48:145
25. Dahn JR, Sacken U, Michal CA (1990) Solid State Ion 44:87
26. Lian F, Gao M, Qiu WH, Axmann P, Mehrens MW (2012) J Appl Electrochem 42:409
27. Hong YJ, Kim JH, Kim MH, Kang YC (2012) Mater Res Bull 47:2022